Available online at www.sciencedirect.com
ScienceDirect
Biochimica et Biophysica Acta 1778 (2008) 917–930
Biochimica et Biophysica Acta
BBA
www.elsevier.com/locate/bbamem

Ceramides modulate cell-surface acetylcholine receptor levels

C.E. Gallegos, M.F. Pediconi, F.J. Barrantes *

UNESCO Chair of Biophysics and Molecular Neurobiology and Instituto de Investigaciones Bioquímicas de Bahía Blanca, C.C. 857, B8000FWB Bahía Blanca, Argentina

Received 12 July 2007; received in revised form 25 September 2007; accepted 19 October 2007
Available online 30 October 2007

Abstract

The effects of ceramides (Cer) on the trafficking of the nicotinic acetylcholine receptor (AChR) to the plasma membrane were studied in CHO-K1/A5 cells, a clonal cell line that heterologously expresses the adult murine form of the receptor. When cells were incubated with short- (C_6-Cer) or long- (brain-Cer) chain Cer at low concentrations, an increase in the number of cell-surface AChRs was observed concomitant with a decrease in intracellular receptor levels. The alteration in AChR distribution by low Cer treatment does not appear to be a general mechanism since the surface expression of the green fluorescent protein derivative of the vesicular stomatitis virus protein (VSVG-GFP) was not affected. High Cer concentrations caused the opposite effects, decreasing the number of cell-surface AChRs, which exhibited higher affinity for [^{125}I]-α-bungarotoxin, and increasing the intracellular pool, which colocalized with *trans*-Golgi/TGN specific markers. The generation of endogenous Cer by sphingomyelinase treatment also decreased cell-surface AChR levels. These effects do not involve protein kinase Cζ or protein phosphatase 2A activation. Taken together, the results indicate that Cer modulate trafficking of AChRs to and stability at the cell surface.

Keywords: Nicotinic receptor; Ceramide; Sphingosine; Protein traffic; Sphingomyelinase

1. Introduction

Studies from various laboratories, including ours, have demonstrated the importance of lipids in the homeostasis and ion channel function of the nicotinic acetylcholine receptor (AChR) (see reviews in Refs. [1–3]). In particular, sphingolipids (SLs) and cholesterol (Chol) intervene in the regulation of the trafficking and cell-surface expression of the AChR [3]. Thus, the decrease in Chol or SL levels induces changes in the distribution of AChRs, diminishing the number of surface receptors [4,5] and augmenting their retention at intracellular compartments [6]. In the case of SLs, it has been demonstrated that impaired biosynthesis results in lower levels of cell-surface AChR [7], which can be accounted for by the impairment of AChR assembly and sequestration of unassembled forms in the endoplasmic reticulum (ER) [8]. The importance of SLs in the regulation of protein traffic is well documented. In yeast, alterations in the synthesis of SL result in defects in the trafficking of the "raft"-resident protein Fus-Mid-GFP from the *trans*-Golgi network (TGN) to the plasma membrane. Newly synthesized cell-surface proteins have been postulated to travel through compartments containing qualitatively and quantitatively different SLs, and alteration of their levels could influence protein transport [9,10]. Until the late 1970s, sphingomyelin (SM) was considered an inert structural lipid, mainly concentrated in the outer layer of the plasma membrane. In recent years the emergence of SLs and other lipids as important second messengers has been documented [11]. Degradation of SM by activation of sphingomyelinase (SMase) initiates a series of reactions that ends in specific cellular responses ultimately mediated e.g. by the biosynthetic precursor of SM, ceramide (Cer). Probable targets for Cer action are Cer-activated protein phosphatase 2A (PP2A) [12], a Cer-activated protein kinase [13], the guanine-nucleotide exchange factor Vav [14] and the protein kinase Cζ (PKCζ) isoform [15–17]. Other reported effects of Cer are concerned with the promotion of

Abbreviations: AChR, nicotinic acetylcholine receptor; Cer, ceramides; CHO, Chinese hamster ovary; Chol, cholesterol; ER, endoplasmic reticulum; Gal-T, galactosyltransferase; GFP, green fluorescence protein; GlcCer, glucosylceramide; LDH, lactate dehydrogenase; RFP, red fluorescent protein; SLs, sphingolipids; SM, sphingomyelin; SMase, sphingomyelinase; TGN, *trans*-Golgi network; VSVG, vesicular stomatitis virus protein; YFP, yellow fluorescent protein; αBTX, α-bungarotoxin

* Corresponding author. Tel.: +54 291 4861201; fax: +54 291 4861200.
E-mail address: rtfjb1@criba.edu.ar (F.J. Barrantes).

0005-2736/$ - see front matter © 2007 Elsevier B.V. All rights reserved.
doi:10.1016/j.bbamem.2007.10.019

changes in the biophysical properties of membranes. SLs and Chol have been postulated to occur in laterally segregated lipid microdomains termed "rafts" [18], suggested to concentrate signaling molecules and receptors in particular regions of the cell surface [19,20]. Recent studies indicate that Cer are able to compete with Chol for association with ordered domains in lipid bilayers [21,22].

In this study we analyzed the effects exerted by Cer on different properties of the paradigmatic neurotransmitter receptor, AChR, using CHO-K1/A5, a Chinese hamster ovary clonal cell line developed in our laboratory that stably expresses the adult form ($\alpha_2\beta\delta\varepsilon$) of the murine muscle AChR [7]. Short- (synthetic C_6-Cer) or long- (natural, from bovine brain) chain Cer at concentrations of 5 μM were found to increase AChRs at the cell surface with a concomitant decrease in intracellular receptor levels. Higher Cer concentrations (25–37.5 μM) caused the opposite effects. In addition, we observed an increment in the affinity of the surface AChRs for the specific competitive antagonist αBTX. Sphingosine, a lipid structurally and metabolically related to Cer, did not produce any significant changes in surface receptors levels, pointing to the specificity of the effect exerted by Cer. The endogenous generation of Cer by SMase treatment also diminished cell-surface AChRs, albeit through a different mechanism. Taken together, our findings indicate that the exocytic transport of the AChR can be homeostatically modulated by Cer which augment or decrease AChR delivery to the cell surface depending on the Cer concentration.

2. Materials and methods

2.1. Materials

C_6-ceramides (C_6-Cer) were purchased from Matreya (Pleasant Gap, Pennsylvania, USA). α-Bungarotoxin (αBTX), D-tubocurarine (d-TC), carbamoylcholine hydrochloride, nystatin, natural ceramides (from bovine brain, brain-Cer), sphingosine, sphingomyelinase (SMase) from *Bacillus cereus*, okadaic acid, PKCζ pseudo-substrate, mouse monoclonal anti-AChR antibody mAb 210 and bovine albumin (fraction V, cell culture tested), were from Sigma Chemical Company (St. Louis, MO, USA). Nutridoma-SP medium with controlled lipid content was purchased from Boehringer Ingelheim, Germany. Iodinated α-bungarotoxin ([^{125}I]-αBTX) was purchased from New England Nuclear (Boston, Mass., USA). Alexa Fluor^{488}-conjugated αBTX (Alexa Fluor^{488}-αBTX), Alexa Fluor^{594}-αBTX, C_6-NBD-ceramide and C_5-BODIPY-SM were from Molecular Probes, OR, USA. The mouse monoclonal anti-syntaxin 6 antibody was from Stressgen Biotechnologies Corporation, Victoria, BC, Canada. Alexa Fluor^{488} F (ab′)$_2$ fragment of goat anti-mouse IgG was from Molecular Probes, OR, USA. The plasmid coding for the green fluorescence protein-G-protein of the vesicular stomatitis virus (VSVG-GFP) was a gift from Dr. Alfonso Gonzalez, Catholic University, Santiago, Chile. The plasmid of the enhanced yellow fluorescent protein/human β1,4-galactosyltransferase (pEYFP-Gal-T; Clontech Laboratories Inc., Palo Alto, CA, USA) was a gift from Drs. Jennifer Lippincott-Schwartz and George Patterson, NIH. The non-toxic mutant of lysenin conjugated with red fluorescent protein (nt-lysenin-RFP) was a gift from Dr. T. Kobayashi, RIKEN (Institute of Physical and Chemical Research), Japan.

2.2. Cell culture

CHO-K1/A5 cells were grown in Ham's F-12 medium supplemented with glutamine, 40 μg/ml gentamicyn sulphate and 10% bovine fetal serum in a Napco (model 6100) incubator maintained at 37 °C with a 5% CO_2/95% air mixture. After cells reached 70–80% confluence they were washed and cultured for an additional period of 30 min and 1, 3 or 5 h under control conditions or in C_6-Cer-, brain-Cer- or sphingosine-supplemented medium. Short- and long-chain Cer were added as a complex with albumin as reported by Rosenwald and Pagano [23], whereas sphingosine was solubilized in methanol (solvent concentration in the culture medium was kept below 0.2%).

2.3. Sphingomyelinase controlled hydrolysis

This series of experiments were carried out on cells cultured as described above and then subjected to SMase (100 mU/ml) hydrolysis for 1 h at 37 °C in delipidated medium. In some cases, 10 min incubation with 0.1 μM okadaic acid or 2.5 μM PKCζ pseudo-substrate preceded the incubation with SMase. For nystatin treatment, the drug (50 μg/ml) was added in delipidated medium and incubated at 37 °C for 30 min; cells were further incubated for 1 additional hour in the absence or presence of SMase, in the continuous presence of nystatin. In the case of long Cer treatments, CHO-K1/A5 cells were incubated with 5 μM C_6-Cer or brain-Cer for 24 h in Nutridoma-BO medium devoid of serum. Exogenous SM at a final concentration of 10 μM was added to cells as described in a recent work from our laboratory [8] using ethanol:decane (98:2 per vol.) as a vehicle. The latter was kept below 0.16%.

2.4. Equilibrium and kinetic studies of [^{125}I]-α-bungarotoxin binding

Surface AChR expression was determined by incubating 70–80% confluent cells with increasing concentrations (5–60 nM) of [^{125}I]-αBTX in cell culture medium for 1 h at 25 °C. At the end of the incubation period, dishes were washed twice with Dulbecco's phosphate-buffered saline and the cells were removed by scraping and collected with 0.1 N NaOH. The radioactivity was measured in a gamma counter with an efficiency of 80%. Non-specific binding was determined from the radioactivity remaining in the dishes when the cells were first pre-incubated with 10 μM native αBTX or 10 mM carbamoylcholine chloride before addition of [^{125}I]-αBTX. Non-specific binding amounted to 10% in control and treated cells. The metabolic half-life of surface AChR was determined as described previously [24]. Cell cultures were labeled with 10 nM [^{125}I]-αBTX for 1 h at 37 °C, washed twice and incubated for the indicated periods. Non-specific binding was determined as described above for the equilibrium experiments. The half-time of degradation was determined from linear regression analysis of the decay curve. Total AChR was determined after lysis of the cells in 10 mM Tris HCl buffer, pH 7.4, containing 150 mM NaCl, 5 mM EDTA, 1% Triton X-100, 0.02% NaN_3, and 10 μg/ml each chymostatin, leupeptin, pepstatin, tosyl-lysine chloromethyl ketone and tosyl phenylalanine chloromethyl ketone, all added to the buffer immediately before use [25]. Cell extracts were frozen and the binding assay was carried out as described previously [26]. Briefly, the extracts were thawed and 20–40 μl aliquots of the cell lysate were incubated with 10 mM phosphate buffer containing 100 mM NaCl, 1% Triton X-100 and [^{125}I]-αBTX (60 nM) in a final volume of 125 μl. In these cases, non-specific binding was determined in samples treated with 10 mM carbamoylcholine chloride, or boiled for 5 min prior to the binding assay. Non-specific binding obtained by either procedure amounted to 20–30% of the total. The binding reaction was terminated by the addition of 100 μl of the incubation reaction on DE-81 paper dishes (Whatman, Germany). DE-81 papers were washed three times in 10 mM phosphate buffer containing 0.1% Triton X-100 at 10 min intervals. Dried papers were counted in a Beckman gamma counter with 80% efficiency. The internal pool of AChR was calculated as the difference between the total number of [^{125}I]-αBTX binding sites and cell-surface sites. In other experiments, total AChR was determined by brief (5 min) treatment of the cells on the Petri dish with 0.5% saponin in phosphate buffer. The detergent was removed, the cells washed, and AChR levels determined by the standard [^{125}I]-αBTX binding assay [6,7]. The rate of αBTX association was calculated by following the time-dependent formation of [^{125}I]-αBTX–AChR complexes in cells incubated with radioiodinated toxin (10 nM) for different periods.

2.5. Inhibition of initial rates of αBTX binding

Determination of the IC_{50} for the full agonist carbamoylcholine was carried out by measuring the initial rate of [^{125}I]-αBTX binding in the presence of the agonist. Cells were incubated in 800 μl of culture medium plus 100 μl of the

corresponding carbamoylcholine concentration for 30 min at room temperature. [^{125}I]-αBTX was added to the medium at a final concentration of 10 nM and incubation continued for a further 20 min. The medium was then removed and the cells were washed with Dulbecco's buffered saline and solubilized by 0.1 N NaOH.

2.6. Protein content

Protein content was determined by the method of Lowry et al. [27] upon solubilization of cells with 0.1 N NaOH using bovine serum albumin as standard.

2.7. Lactate dehydrogenase activity

In order to evaluate the occurrence of cell damage at high Cer concentrations, the activity of lactate dehydrogenase (LDH) released in the culture medium was determined [28,29] using a UV kinetic assay (Wiener Lab, Rosario, Argentina) that measures the amount of NADH converted to NAD^+. LDH levels from cells disrupted with an ultrasonic homogenizer were used as a control of cellular damage.

2.8. Cell transfection

CHO-K1/A5 cells were transiently transfected with the cDNA coding for the fusion proteins pEYFP-Gal-T and VSVG-GFP using the Polifect transfection reagent (Quiagen Inc. CA, USA). Transfection was performed 24 h before Cer treatment.

2.9. Lipid analysis

In some experiments, C_6-Cer were added to the culture medium as a precursor for the synthesis of SM and glucosylceramide (GlcCer). For this purpose, CHO-K1/A5 cells were cultured in 10 cm culture dishes in the presence of complete medium for one day. They were subsequently washed with sterile phosphate-buffered saline (PBS; 150 mM NaCl, 10 mM Na_2HPO_4, 10 mM NaH_2PO_4, pH 7.4) and Nutridoma-BO medium was added. The cells were then incubated with 5 μM C_6-Cer in the presence of trace concentration (25 nM) of C_6-NBD-Cer at 37 °C for 0.5 and 24 additional hours. Lipid extracts were prepared as previously described [6]. SLs were separated by thin-layer chromatography using silica gel G plates and $CHCl_3$:CH_3OH:H_2O, 65:25:4 (by vol.) as the mobile phase [30,31]. C_6-NBD-Cer and C_5-BODIPY-SM were used as fluorescent standards. Fluorescent lipid spots were detected by UV illumination.

2.10. Fluorescence microscopy

In order to label surface AChRs, cells were incubated with Alexa Fluor^{488}-conjugated αBTX (Alexa Fluor^{488}-αBTX) at a final concentration of 1 μg/ml in PBS, for 1 h, on ice. Excess label was removed by washing with PBS prior to microscopy. To label intracellular AChRs, cell-surface AChRs were first saturated by incubation of CHO-K1/A5 cells with 1 μg/ml native αBTX in PBS for 1 h. Cells were then fixed with 4% paraformaldehyde for 40 min, permeabilized with 0.1% Triton X-100 for 20 min, and incubated with Alexa Fluor^{594}-αBTX at a final concentration of 1 μg/ml for 1 h at room temperature.

For colocalization studies of intracellular AChRs with the TGN marker syntaxin 6, cells were fixed and permeabilized as above, and incubated with primary antibody (mouse anti-syntaxin 6, 1:500) for 1 h at room temperature in PBS containing 1% BSA. Cells were then washed three times with PBS and incubated with secondary fluorophore-conjugated antibody (Alexa Fluor^{488}-goat anti-mouse IgG, 1:5000). Alexa Fluor^{647}-αBTX was added with the secondary antibody to label intracellular AChRs. Incubation was performed at room temperature for 1 h in PBS containing 1% BSA. Cells were washed three times with PBS before coverslips were mounted.

Fluorescence imaging was carried out using a wide-field imaging system (Nikon Eclipse E-600 microscope) accomplished with a SBIG model ST-7 digital charge-coupled device camera (765×510 pixels, 9.0×9.0 μm pixel size, Santa Barbara, CA), thermostatically cooled at −10 °C. The ST-7 CCD camera was driven by the CCDOPS software package (SBIG Astronomical Instruments, version 5.02, Santa Barbara, CA). For all experiments a 60× (1.4 N.A.) oil-immersion objective was used. Appropriate dichroic and emission filters were employed to avoid crossover of fluorescence emission. Confocal images were acquired with a Leica TCS SP2 microscope (Leica Microsystems Heidelberg GmbH).

2.11. Quantitative analysis of fluorescence microscopy images

Fluorescence images were analyzed with the software Scion Image version 4.0.2 (Scion Corp., Frederick, MD). Fluorescence intensities were measured in 8-bit images by selecting small membrane areas (cell-surface AChR) or by delimiting the whole cell (intracellular AChR). Fluorescence intensity values were corrected for background fluorescence. The average fluorescence intensity over distinct areas of the cell surface was calculated for randomly chosen cells for each experimental condition. For illustration purposes, images were processed using Adobe Photoshop 5.5, scaled with identical parameters, and pseudo-colored according to the corresponding emission wavelength.

2.12. Evaluation of unassembled AChR by fluorescence microscopy

Unassembled AChR was determined using a fluorescence microscopy assay based on agonist inhibition of αBTX binding recently introduced by our laboratory [8]. Briefly, cell-surface AChRs were blocked with native toxin, fixed, permeabilized and incubated with 10 mM carbamoylcholine for 1 h at room temperature, and subsequently incubated with Alexa^{594}-αBTX in the presence of agonist. As a control for total intracellular AChR, cells were incubated with PBS instead of agonist for the same period. Quantitative measurements of fluorescence intensities of intracellular AChR label in the presence and absence of agonist provided an estimation of the amount of unassembled AChR.

2.13. AChR internalization studies

Surface AChRs were labeled with Alexa^{488}-αBTX at 4°C as described above, followed by incubation at 37 °C for increasing periods (from 0 to 4 h) in the presence or absence of SMase. The fluorescence intensity at the cell surface and the ratio of surface to total AChR was calculated for each incubation time. In some cases, a double-labeling protocol was carried out as in Borroni et al. [4]. Cells were first labeled with Alexa^{647}-αBTX (far red) at 4 °C (to arrest receptor internalization) and then incubated at 37 °C for 0 and 1 h, respectively, to re-establish endocytic processes. To reveal those AChRs remaining at the cell surface, cells were then labeled with mAb 210 (which recognizes an extracellular epitope of the α1 AChR subunit) at 4 °C, and subsequently labeled with Alexa^{488}-labeled secondary antibody (green).

2.14. Fluorescence microscopy of membrane sheets

For preparation of membrane sheets, CHO-K1/A5 cells were grown on polylysine-coated glass coverslips and disrupted as described previously [4,5] using a 300 ms ultrasound-pulse in ice-cold KGlu buffer (20 mM Hepes, pH 7.2, containing 120 mM potassium glutamate and 20 mM potassium acetate). In the case of SM hydrolysis, membrane sheets were incubated for 30 min at 37 °C in KGlu buffer containing 100 mU/ml SMase, followed by washing with ice KGlu buffer. Control sheets were incubated with only KGlu buffer. They were then double-stained with 1 μg/ml Alexa^{488}-αBTX, and nt-lysenin-RFP for 60 min at 4 °C in KGlu buffer, washed 2–3 times with KGlu buffer, fixed for 30 min in PBS containing 4% PFA, and washed with PBS. Finally, membrane sheets were labeled with 25 μl/ml of a saturated TMA-DPH solution in PBS, in order to identify membrane sheets avoiding preferential selection according to their staining intensity in the Alexa^{488}-αBTX (green) or in the nt-lysenin-RFP (red) channel.

2.15. Lysenin labeling of cell-surface SM

The localization and distribution of cell-surface SM of control and SMase-treated cells were evaluated using lysenin, a fluorescent probe that specifically binds to SM [32]. We used a non-toxic mutant of lysenin conjugated with red fluorescent protein (nt-lysenin-RFP) [33]. After 1 h incubation in the presence or

absence of SMase, cells were washed and incubated with lysenin (1/50 in PBS) for 1 h on ice. The fluorescence intensity of lysenin-labeled SM at the cell surface was quantified by fluorescence microscopy.

2.16. Endogenous generation of C_5-BODIPY-Cer

Direct observation of endogenously generated Cer was accomplished using fluorescence microscopy. First cells were incubated with 15 nM C_5-BODIPY-SM in Ham's F-12 medium devoid of serum for 30 min on ice to label the plasma membrane of CHO-K1/A5 cells. Upon washing with PBS to remove unbound C_5-BODIPY-SM, cells were incubated for 5 min at 37 °C in the absence or presence of bacterial SMase [34].

2.17. Data analysis

Data obtained from saturation isotherms, as well as the transformed Scatchard plots, association kinetic, displacement experiments, and half-life of the cell-surface receptor were analyzed using the Origin 5 software from Origin Lab Corporation. Statistically significant differences were determined by the Student's *t*-test (two-tailed).

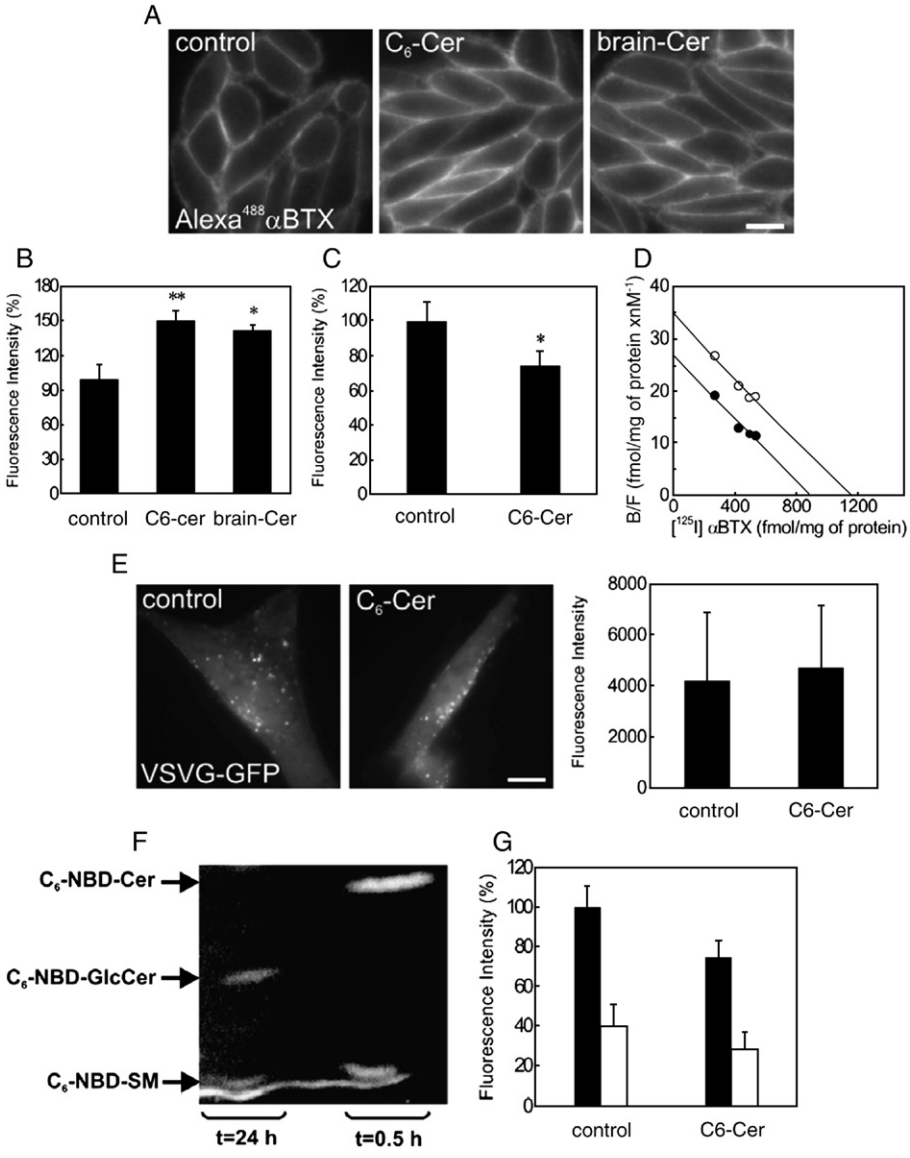

Fig. 1. Incubation with low Cer concentrations increases the number of cell-surface AChRs with concomitant diminution of the intracellular receptor pool. A) Cells incubated for 24 h under control conditions (left panel), 5 μM C_6-Cer (middle panel) or 5 μM brain-Cer (right panel) were labeled with Alexa^{488}-αBTX for 1 h at 4 °C. B) Fluorescent signal of Alexa Fluor^{488}-αBTX arising from surface AChR of control CHO-K1/A5 cells or those treated with 5 μM Cer for 24 h. $^{**}p<0.01$ and $^{*}p<0.05$. C) Quantification of intracellular receptors labeled with Alexa Fluor^{594}-αBTX in cells treated with 5 μM C_6-Cer. $^{*}p<0.05$. D) Scatchard plots of specific [^{125}I]-αBTX binding in control CHO-K1/A5 cells (●) and in cells incubated with 5 μM C_6-Cer (○). E) Fluorescence images of VSVG-GFP fluorescence in cells grown either under control conditions (left panel) or in the presence of 5 μM C_6-Cer for 24 h (right panel). Bars represent the quantification of VSVG-GFP fluorescent signal at the cell surface. $^{*}p<0.01$. Scale bar: 10 μm. F) Endogenous generation of fluorescent SM and glucosylceramide species upon incubation of CHO-K1/A5 cells with C_6-NBD-Cer. CHO-K1/A5 cells were incubated with 5 μM C_6-Cer+C_6-NBD-Cer for 0.5 h or 24 h. Lipids were extracted and C_6-NBD-Cer metabolites were separated by TLC as described in Materials and methods. C_5-BODIPY-SM and C_6-NBD-Cer were used as fluorescent standards. Chromatogram was photographed under UV light. G) The increment in cell-surface AChR exerted by 5 μM Cer is not due to receptor assembly enhancement. Total (assembled+unassembled=filled bars) and unassembled (empty bars) intracellular AChR in control and CHO-K1/A5 cells treated with 5 μM C_6-Cer for 24 h. Unassembled α subunits were determined by preincubation with 10 mM carbamoylcholine before labeling with Alexa Fluor^{594}-αBTX. Values are expressed as percentage of total control AChR.

3. Results

3.1. Low Cer concentrations increase cell-surface AChR and reduce the number of intracellular receptors

In order to evaluate whether Cer affect the distribution of the AChR, CHO-K1/A5 cells (a clonal CHO cell line expressing the adult form of the AChR) were incubated for 24 h in lipid-deficient medium (Nutridoma-BO) in the presence of short (C_6) Cer at a final concentration of 5 μM and wide-field fluorescence microscopy was used to study the distribution of the AChR. Surface AChRs were labeled with the fluorescent derivative of αBTX, Alexa Fluor^{488}-αBTX (green), and intracellular receptors were visualized by Alexa Fluor^{594}-αBTX (red) staining. C_6-Cer-treated cells showed a marked (~50%) increase in cell-surface Alexa Fluor^{488}-αBTX green fluorescence (Fig. 1A–B), whereas the intracellular red fluorescence showed a ~28% diminution with respect to controls (Fig. 1C).

Although short-chain Cer (C_2-Cer) are found in nature together with long *N*-acyl chain Cer [35], the effects exerted by the former might differ from those induced by long-chain species (see review in Ref. [36]). We therefore compared the results obtained with C_6-Cer with those produced with the more common and naturally occurring long-chain Cer, using a complex mixture of long-chain Cer from bovine brain. As shown in Fig. 1A–B, brain-Cer also increased (~42%) surface AChR as assessed by fluorescence microscopy.

Experiments using [^{125}I]-αBTX were conducted next to determine whether Cer treatment affected the equilibrium binding of this competitive antagonist. The B_{max} for the cell-surface AChR obtained from Scatchard analysis was 40% higher in C_6-Cer-treated cells (from 886 fmol/mg protein in control cells to 1158 fmol/mg protein in Cer-treated cells; Fig. 1D), in full agreement with the fluorescence microscopy experiments (Fig. 1A–B). The increment in cell-surface AChR induced by C_6-Cer was not accompanied by changes in the Kd_{app} for [^{125}I]-

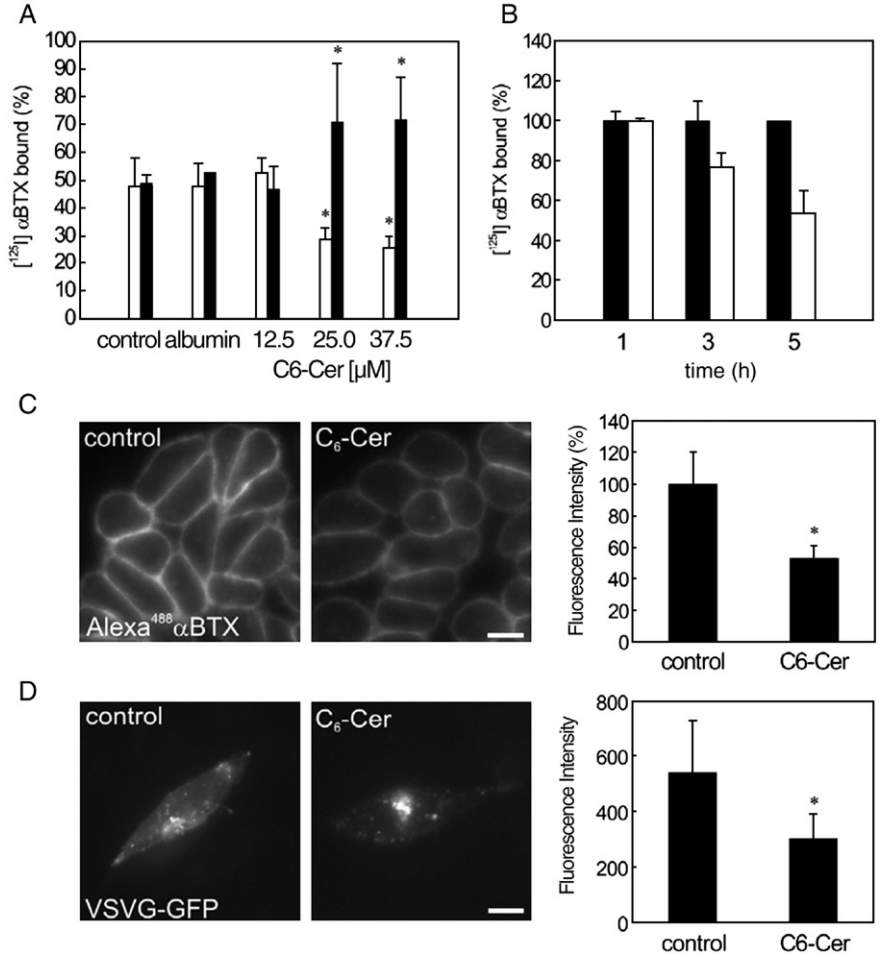

Fig. 2. *Distribution of AChR in CHO cells*. A) Percentage of cell-surface (empty bars) and intracellular [^{125}I]-aBTX binding sites (filled bars) in CHO-K1/A5 cells incubated for 5 h under different experimental conditions. Total receptor corresponds to [^{125}I]-αBTX binding sites upon detergent solubilization of CHO-K1/A5 cells (or upon saponin permeabilization); the intracellular pool was calculated as the difference between the total and cell-surface AChR. Cells were incubated in complete Ham F-12 medium plus bovine serum (control), in serum-free medium plus albumin, or in the latter medium supplemented with 12.5, 25, or 37.5 μM of C_6-Cer. Data are mean values ± SD of five different samples from at least two separate experiments. B) Time-dependence of C_6-Cer inhibition of cell-surface [^{125}I]-αBTX binding, shown here for the highest concentration of the exogenous lipid. Data shows the percentage values obtained after treatment (empty bars) with respect to that found in control cells (filled bars). C) Cell-surface fluorescence of Alexa Fluor^{488}-αBTX-labeled receptors in control and CHO-K1/A5 cells treated with 37.5 μM C_6-Cer for 5 h. *p<0.0001. D) Fluorescence microscopy images of VSVG-GFP expressed in control (left panel) and 37.5 μM C_6-Cer-treated (right panel) CHO-K1/A5 cells. Bars represent the quantification of VSVG-GFP fluorescent signal at the cell surface. Scale bar: 10 μm.

αBTX, indicating that the absolute number of receptors, but not their affinity, was affected by 24 h Cer treatment (Fig. 1D).

In order to determine whether Cer treatment affected the trafficking of proteins other than the AChR, CHO-K1/A5 cells were transfected with the cDNA coding for the vesicular stomatitis virus G protein-green fluorescent protein VSVG-GFP. This fluorescent protein is an efficient probe for following the fate of integral membrane proteins along the exocytic pathway [37]. Transfected CHO-K1/A5 cells were subsequently incubated with 5 μM C_6-Cer and the surface expression of VSVG-GFP was quantified. We observed no significant differences between the surface fluorescent signal of VSVG-GFP of control and Cer-treated cells, indicating that the alteration in the AChR traffic by low Cer treatment was not a general mechanism (Fig. 1E).

In order to identify the lipid species generated upon 24 h incubation with 5 μM C_6-Cer in the presence of trace concentrations of C_6-NBD-Cer, cells were submitted to Folch lipid extraction and subsequent TLC separation with the solvent system described by Lipsky and Pagano [30]. After 0.5 h incubation, C_6-NBD-SM was observed in the thin-layer chromatograms. However, the fluorescent spot corresponding to C_6-NBD-Cer was still present. After 24 h incubation, C_6-NBD-SM and C_6-NBD-GlcCer fluorescent bands could be visualized, whereas the C_6-NBD-Cer were no longer present (Fig. 1F).

As recently reported by Baier and Barrantes [8] the addition of exogenous SM to the culture medium of CHO-K1/A5 cells caused a 3-fold increase in the number of AChRs present at the plasma membrane (data not shown).

3.2. The increase in cell-surface AChR by 5 μM Cer does not involve enhanced receptor assembly

In order to determine whether the augmented cell-surface AChR levels were due to enhanced AChR assembly after a long period (24 h) of Cer incubation, unassembled receptors were measured next using a fluorescence microscopy assay recently introduced by our laboratory [8]. In control cells the percentage of unassembled α subunits was ~40%, diminishing to ~30% in Cer-treated cells (Fig. 1G). Since the total amount of intracellular AChR in Cer-treated cells is lower, as judged by the fainter intensity of the fluorescence signal (Fig. 1C) (which corresponds to the sum of assembled+unassembled intracellular AChRs, Fig. 1G) the ratio of total/unassembled AChR in Cer-treated cells did not differ from the control cells.

3.3. Treatment with high short-chain ceramide (C_6-Cer) concentrations decreases cell-surface AChR and increases the intracellular receptor pool

We next evaluated the effects of increasing Cer concentrations on AChR distribution. Exposure of CHO-K1/A5 cells for periods of up to 5 h with concentrations of C_6-Cer of 12.5 μM

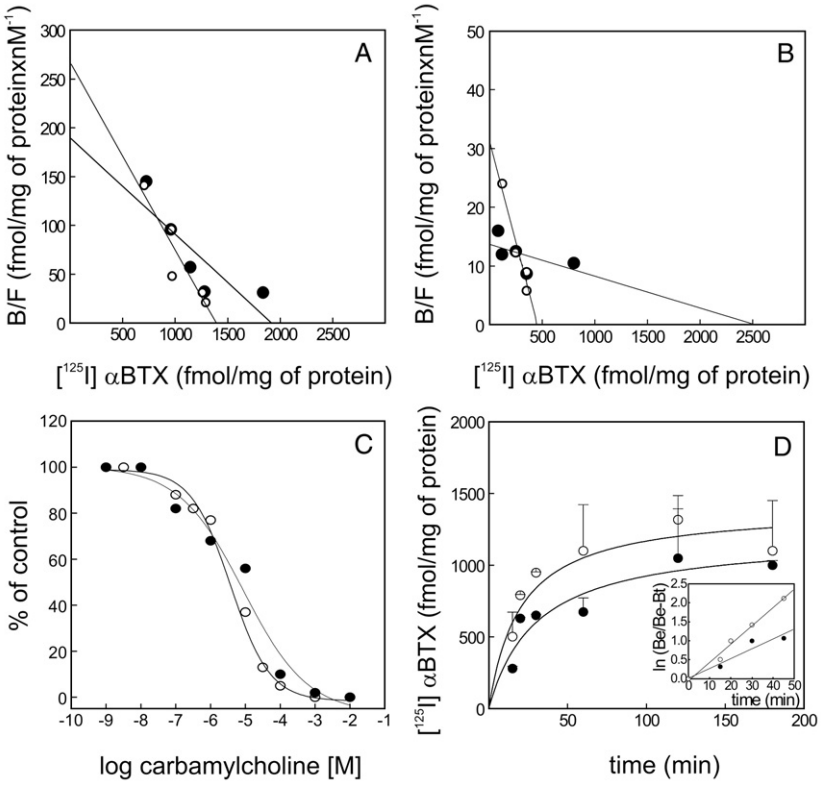

Fig. 3. *Pharmacological characterization of AChR from control and C_6-Cer-treated cells*. A–B) Scatchard plots obtained with the specific binding of radioiodinated αBTX in control (●) and CHO-K1/A5 cells incubated in the presence of 25 μM of C_6-Cer (○) (A) and those incubated under control and 37.5 μM C_6-Cer (B). C) Displacement curves of the total radioactive αBTX binding promoted by the presence of the indicated carbamoylcholine concentrations from control and cells incubated with 37.5 μM C_6-Cer. D) Association kinetics of αBTX to AChR for both of the later conditions. Inset: linearization of the association curves in (D).

did not affect the binding of the competitive antagonist [^{125}I]-αBTX (Fig. 2A). However, incubations with 25 and 37.5 μM C_6-Cer resulted in a decrease in cell-surface AChR with a concomitant increase in the intracellular AChR pools (Fig. 2A), without significant changes in the total amount of AChR. This effect was time-dependent (Fig. 2B); cell-surface AChR decreased to 77±7 and 54±11% of control values at 3 and 5 h, respectively. Since short-chain Cer have been postulated to produce damage in some cell systems [38], a series of experiments were carried out to evaluate this possibility using a well known test, the assay of the cytosolic enzyme LDH [28,29]. No significant differences were detected in LDH levels between control cells and cells incubated with 37.5 μM of C_6-Cer for 3 and 5 h at 37 °C (Supplementary Fig. 1).

Fluorescence microscopy experiments were performed in parallel to study the distribution of AChR in Cer-treated CHO-K1/A5 cells. A 46% reduction in cell-surface Alexa Fluor^{488}-αBTX fluorescence was observed in cells treated with 37.5 μM C_6-Cer with respect to controls (Fig. 2C). The surface expression of the fusion protein VSVG-GFP was also significantly reduced (~45%) by this treatment (Fig. 2D) indicating that Cer treatment at high concentrations affected the traffic of other proteins besides the AChR.

We next evaluated whether high Cer concentration affected the affinity of the AChR–αBTX complex formation. C_6-Cer produced an increase in [^{125}I]-αBTX affinity for the AChR in addition to a reduction in the density of cell-surface receptor (Fig. 3A–B). The higher affinity of the AChR upon Cer treatment was also apparent in competition experiments using the full agonist carbamoylcholine (Fig. 3C). The apparent equilibrium dissociation constant of those AChRs remaining at the cell surface upon Cer treatment decreased by ~50% and ~60% in cells treated with 25 and 37.5 μM C_6-Cer, respectively. This change in affinity could be accounted for by the corresponding changes in the kinetics of [^{125}I]-αBTX binding to cell-surface AChR, which also showed statistically significant differences between Cer-treated and control cells. As shown in Fig. 3D, the rate of association between toxin and AChR increased upon Cer treatment. Thus, the decrease in cell-surface AChR levels cannot be accounted for by a decrease in affinity for the competitive antagonist αBTX.

3.4. C_6-Cer treatment arrests AChR at the exiting end of the Golgi complex

Treatment with 37.5 μM C_6-Cer for 5 h increased intracellular Alexa Fluor^{594}-αBTX fluorescence by ~50% (Fig. 4A). The pattern of intracellular fluorescence also changed: whereas in control cells the AChR was quite uniformly distributed over the entire cell, a higher fluorescence intensity was observed at the perinuclear region in cells treated with C_6-Cer (Fig. 4B). Since this pattern was reminiscent of the *trans*-Golgi network (TGN), identified in a previous work from our laboratory as the subcellular compartment where AChR is arrested upon impairment of Chol biosynthesis [6], cells were also transiently transfected with the pEYFP-Golgi vector, which codifies for the fusion

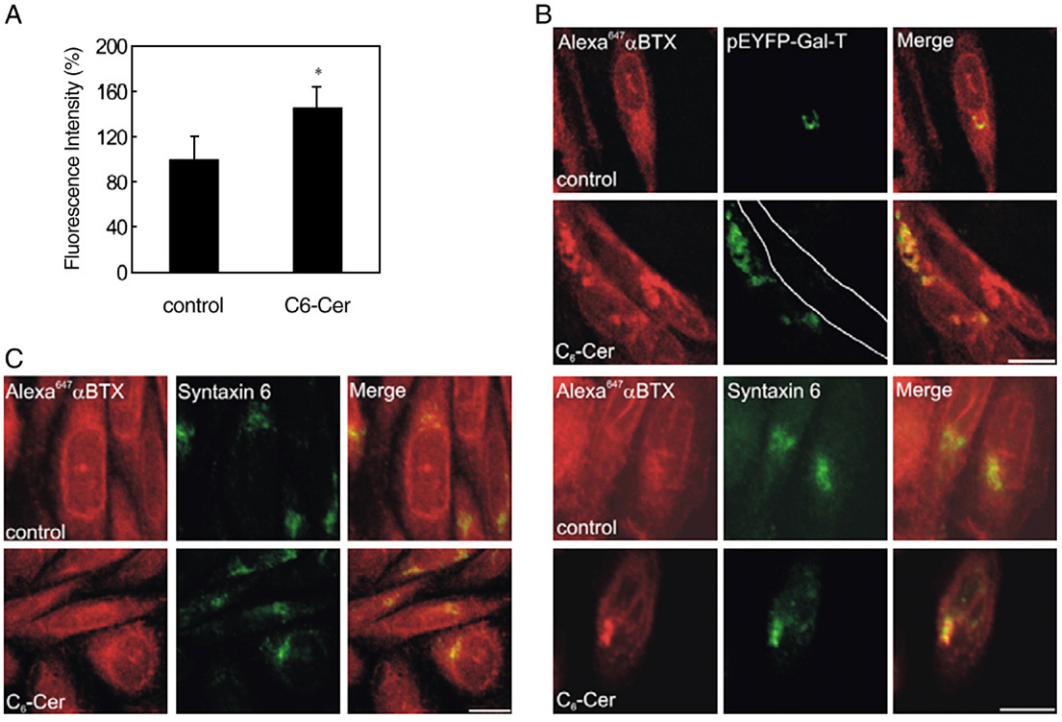

Fig. 4. *High C_6-Cer concentrations increase the intracellular pool of AChR and change its intracellular distribution.* A) Percentage of intracellular receptors labeled with Alexa Fluor^{594}-αBTX in CHO-K1/A5 cells incubated under control conditions or in the presence of 37.5 μM C_6-Cer for 5 h. *$p<0.001$. B) Colocalization of intracellular Alexa Fluor^{647}-αBTX-labeled-receptors (left panel) with the *trans*-Golgi/TGN markers pEYFP-Gal-T and syntaxin 6 (middle panel) in control and 37.5 μM Cer-treated cells. Merged images are given in the right panel. Scale bar: 10 μm. C) Colocalization of intracellular Alexa Fluor^{647}-αBTX-labeled-receptors (left panel) with syntaxin 6 (middle panel) in cells treated with 5 μM Cer. Right panel: merged images. Scale bar: 10 μm.

protein pEYFP-Gal-T. Gal-T is a well known marker of the TGN [39,40]. Twenty-four hours after transfection the cells were incubated with 37.5 μM C_6-Cer for 5 h and intracellular AChRs were labeled with Alexa Fluor^{647}-αBTX. Confocal microscopy images revealed an important degree of colocalization of the fluorescent signals arising from intracellular-labeled AChRs and the TGN marker (Fig. 4B). As a specific marker of the TGN [41], the anti-syntaxin 6 antibody yielded similar colocalization with AChRs (Fig. 4B). Thus, treatment with high C_6-Cer concentrations appears to block trafficking of the AChR to the cell surface and result in the accumulation of the AChR at the exiting end of the Golgi complex. On the other hand, incubation with low C_6-Cer concentrations (5 μM) did not induce any changes in the intracellular distribution of the AChR nor in the structure of the TGN as evaluated by anti-syntaxin 6 labeling (Fig. 4C).

3.5. Long-chain Cer mimic the effect of short-chain Cer on AChR distribution whereas sphingosine does not

Binding experiments with [^{125}I]-αBTX were carried out to test the effect of long-chain Cer on AChR distribution. After 5 h treatment long-chain brain-Cer (37.5 μM) were also found to reduce surface AChR and increase intracellular receptors (Table 1). A similar reduction of cell-surface AChR (~40%) was observed in Alexa Fluor^{488}-αBTX fluorescence microscopy experiments (Fig. 5A–B), with a concomitant increase in intracellular Alexa Fluor^{594}-αBTX fluorescence (Fig. 5C).

Since Cer can be rapidly converted to sphingosine [42], it was necessary to confirm that it was Cer and not sphingosine which exerts the cellular effect. For this purpose we evaluated whether sphingosine produced changes in AChR distribution analogous to those detected with Cer. Under conditions similar to those used for Cer experiments, sphingosine did not affect surface or intracellular AChR (Table 2).

3.6. Endogenously generated Cer also diminish cell-surface AChR levels

We next asked the question whether endogenous generation of Cer affects surface expression of the AChR. For this purpose CHO-K1/A5 cells were incubated with 100 mU/ml of bacterial SMase for 1 h at 37 °C. [^{125}I]-αBTX binding assays showed that cell-surface AChR decreased by ~35% in SMase-treated cells (Fig. 6A). Similar results were obtained using the Alexa Fluor^{488}-αBTX fluorescence microscopy assay (Fig. 6B).

Table 1
Effects of brain-Cer on the surface, intracellular and total AChR in CHO-K1/A5 cells

Condition	Surface	Intracellular	Total
Control (6)	527±27	571±140	1098±285
Albumin 3 h (5)	524±4	579±104	1103±199
Brain-Cer 3 h (5)	369±45**	629±159	998±252
Albumin 5 h (7)	532±80	577±115	1109±167
Brain-Cer 5 h (7)	285±106**	462±95	747±154*

Results are mean values±SD expressed as fmol of [^{125}I]-αBTX specifically bound/mg protein. Numbers between parentheses are the number of individual samples analyzed. *$p<0.025$; **$p<0.001$.

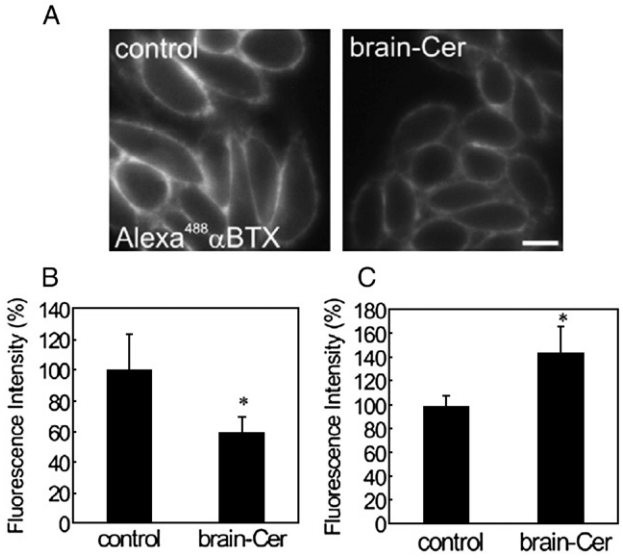

Fig. 5. *Brain-Cer affect the AChR distribution in CHO-K1/A5 cells*. Cells were grown either in control medium or in the presence of 37.5 μM brain-Cer for 5 h. A) Fluorescence microscopy images of surface receptors labeled with Alexa Fluor^{488}-αBTX in control (left panel) and Cer-treated cells (right panel). Scale bar: 10 μm. B) Percentage of Alexa Fluor^{488}-αBTX fluorescent signal at the cell surface. *$p<0.001$. C) Histograms quantifying intracellular receptors labeled with Alexa Fluor^{594}-αBTX. Fluorescence was quantified as described in Materials and methods. *$p<0.0001$.

Since Cer have been implicated in the activation of PP2A [12,43], and subunit assembly, insertion and stability of the AChR at the cell membrane have been reported to be affected by the state of receptor phosphorylation [44–47], we studied next whether PP2A was involved in the retention of AChR at intracellular compartments. Incubation with 0.1 μM okadaic acid, a well known inhibitor of the Cer-activated PP2A [48], did not reverse the diminution in AChR surface fluorescence signal produced by SMase treatment (Supplementary Fig. 2).

The ζ isoform of the enzyme protein kinase C (PKCζ) has also been reported to be activated by Cer [49]. To analyze the possibility that PKCζ was involved in the Cer-induced alteration of AChR traffic, the specific inhibitor PKCζ pseudo-substrate was tested. Similar to what was observed with okadaic acid, this inhibitor was not able to revert the effects of SMase treatment on surface AChR levels (data not shown).

An independent assay of SMase action exploited the fluorescent dye nt-lysenin-RFP. Lysenin is an earthworm toxin that specifically recognizes SM-rich membrane domains and induces cytolysis by pore formation [50]. The specific binding of

Table 2
Effects of sphingosine on the surface and intracellular AChR expressed in CHO-K1/A5 cells

Condition	Surface	Intracellular	Total
Control (6)	527±27	571±140	1208±121
MeOH 5 h (13)	550±33	549±11	1099±22
Sphingosine 5 h (12)	511±66	619±92	1130±170

Results are mean values±SD expressed as fmol/mg protein. The effect of sphingosine was determined after 5 h treatment with 37.5 μM SM. Other details are as in Table 1.

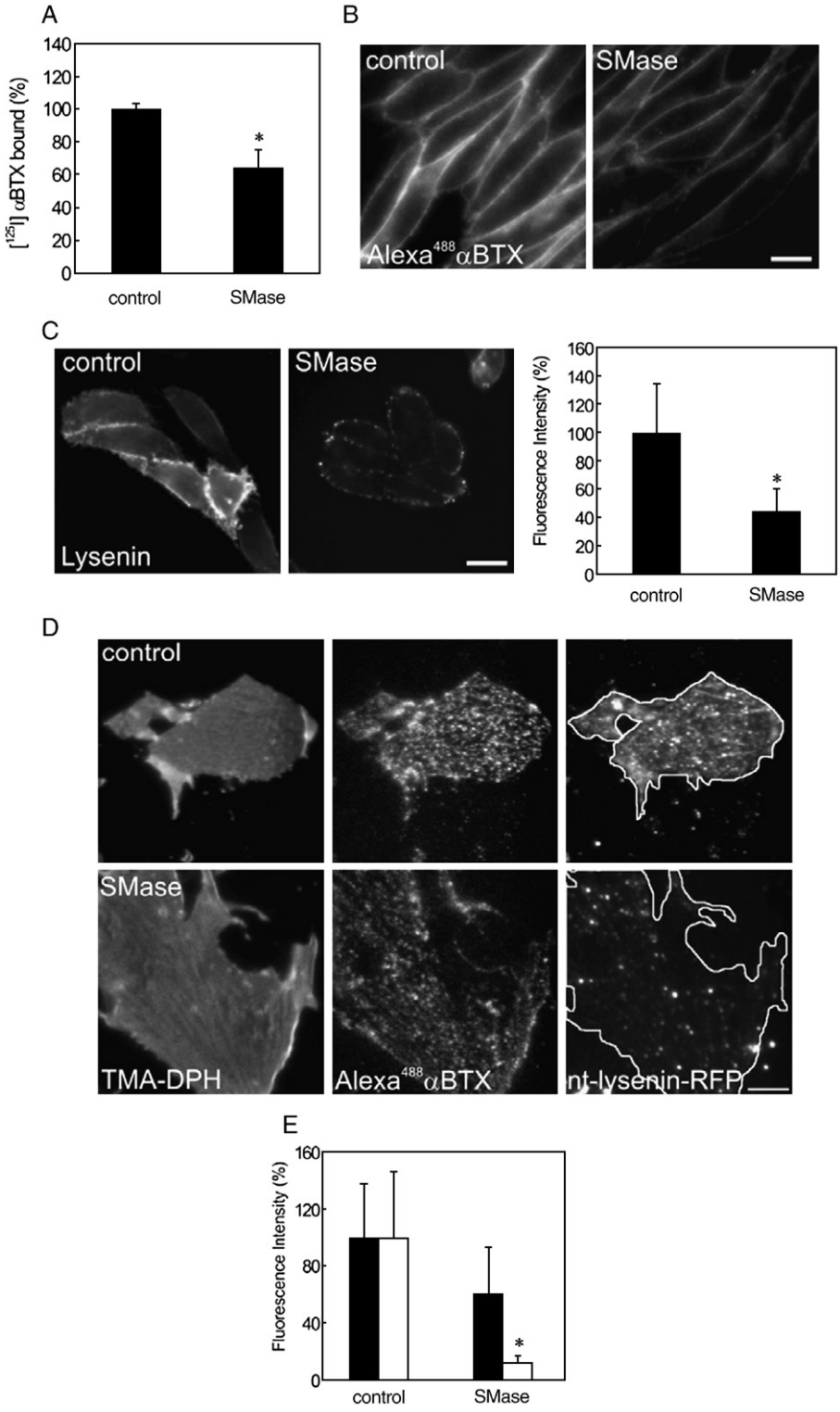

Fig. 6. *Endogenous generation of Cer also decreases surface AChR*. A) Percentage of cell-surface [^{125}I]-αBTX binding sites in CHO-K1/A5 cells incubated for 1 h either under control conditions or in the presence of SMase 100 mU/ml. *$p<0.005$. B) Cell-surface fluorescence of Alexa^{488}-αBTX-labeled receptors in control (left panel) and SMase-treated (right panel) cells. Scale bar: 10 μm. C) Plasma membrane SM labeled with the fluorescent dye nt-lysenin-RFP in control and SMase-treated cells. *$p<0.0001$. Scale bar: 10 μm. D) Fluorescence microscopy images of control and SMase-treated membrane sheets obtained as described in Materials and methods, and labeled with TMA-DPH (left panel), Alexa^{488}-αBTX (middle panel) and nt-lysenin-RFP (right panel). Scale bar: 5 μm. The perimeter of the membrane sheets is outlined in the nt-lysenin-RFP panels to facilitate visualization. E) Percentage of Alexa^{488}-αBTX (filled bars) and nt-lysenin-RFP (empty bars) fluorescence in membrane sheets incubated in the absence (control) or in the presence of bacterial SMase. *$p<0.001$.

lysenin to SM makes it a useful tool to examine the cell distribution of SM [32]. Here we used the red fluorescent protein adduct of a non-toxic mutant of lysenin, recently developed by Kiyokawa et al. [33]. Only discrete puncta remained at the cell surface after SMase action (Fig. 6C), which reduced the lysenin fluorescence signal by ~55% (Fig. 6C).

In order to visualize the endogenous generation of Cer, cells were labeled with a SM probe, C_5-BODIPY-SM, and subjected to SMase treatment [34]. Upon incubation with SMase for 5 min at 37 °C, a significant fraction of the fluorescent adduct, C_5-BODIPY-Cer, appeared to have been translocated to the Golgi region (Supplementary Fig. 3), in agreement with the results of Pagano et al. [51].

To determine whether the decrease in cell-surface AChR mediated by SMase treatment was a result of the mere physical presence (or absence) of the lipid in the membrane, another series of experiments was conducted on isolated, single-sheets of AChR-containing plasma membranes, exploiting the formation of single-sheets of plasma membranes by ultrasound treatment as recently described in work from our laboratory [4,5]. This treatment results in the "unroofing" of the cells, leaving behind only their glass-adhered, ventral membrane, and eliminates cytosol, organelles and metabolic integrity of the cell. Upon incubation of membrane sheets with SMase for 30 min at 37 °C in KGlu buffer, the specimens were double labeled with Alexa Fluor^{488}-αBTX and nt-lysenin-RFP. TMA-DPH labeling was also performed in order to identify membrane sheets avoiding preferential selection according to their staining intensity in the Alexa^{488}-αBTX or in the nt-lysenin-RFP channel. Whereas no significant differences were observed in the fluorescence signal arising from Alexa Fluor^{488}-αBTX-labeled receptors, a drastic decrease (~90%) in the lysenin fluorescence was apparent (Fig. 6D), suggesting the possibility that the diminution of AChR levels upon SMase treatment requires the integrity of the cell.

3.7. The mechanism of cell-surface AChR diminution in SMase-treated cells is different from that in Cer-treated cells

We have recently reported that Chol depletion by methyl-β-cyclodextrin causes rapid internalization of the AChR in CHO-K1/A5 cells [4]. Since Chol and SM are found in close association in biomembranes, forming microdomains [18,52], the decrease in cell-surface AChR upon SMase treatment observed here could operate through a similar mechanism. To test this hypothesis we assayed the rate of AChR internalization upon SMase-mediated cell-surface SM depletion using a double-labeling protocol as in Ref. [4]: cells were first labeled with Alexa^{647}-αBTX (far red) at 4 °C and then incubated with SMase at 37 °C for 0 and 1 h, respectively. AChRs remaining at the cell surface after these two periods were then labeled with mAb 210 (which recognizes an extracellular epitope of the α AChR subunit) at 4 °C, followed by incubation with Alexa^{488}-labeled secondary antibody (green). In control cells, the signal associated with the AChR was observed almost exclusively at the cell surface, in the form of patchy, spotted fluorescence (Fig. 7). This is due to the aggregation of AChR molecules effected by cross-linking with the bifunctional mAb IgG (see also Ref. [5]). Comparison of control conditions at $t=0$ and $t=1$ h revealed an increase in the overlap of fluorescence signals from "old" (red) and "newly-labeled" (green) AChRs, indicating that a large proportion of AChRs remained at the cell surface after 1 h incubation (Fig. 7A). Only few endocytic vesicles (red) could be seen inside cells after 1 h. In contrast, in SMase-treated cells the fluorescence accumulated in abundant single-colored endocytic vesicles (red) concomitantly with a diminution of the overlap between old and new receptors at the cell surface (Fig. 7A and see Ref. [4]). In order to determine the kinetics of this process, surface AChRs were first labeled with Alexa^{488}-αBTX (green) at 4 °C, followed by incubation with SMase at 37 °C for increasing time periods (from 0 to 4 h). The fluorescence intensity at the cell-surface was measured and the ratio of surface/total AChR was calculated from the time-course of the experiment. The $t_{1/2}$ was found to decrease from 1.7 h in control cells to 1 h in SMase-treated cells (Fig. 7B), indicating that SM depletion by bacterial SMase accelerated AChR internalization kinetics, roughly to the

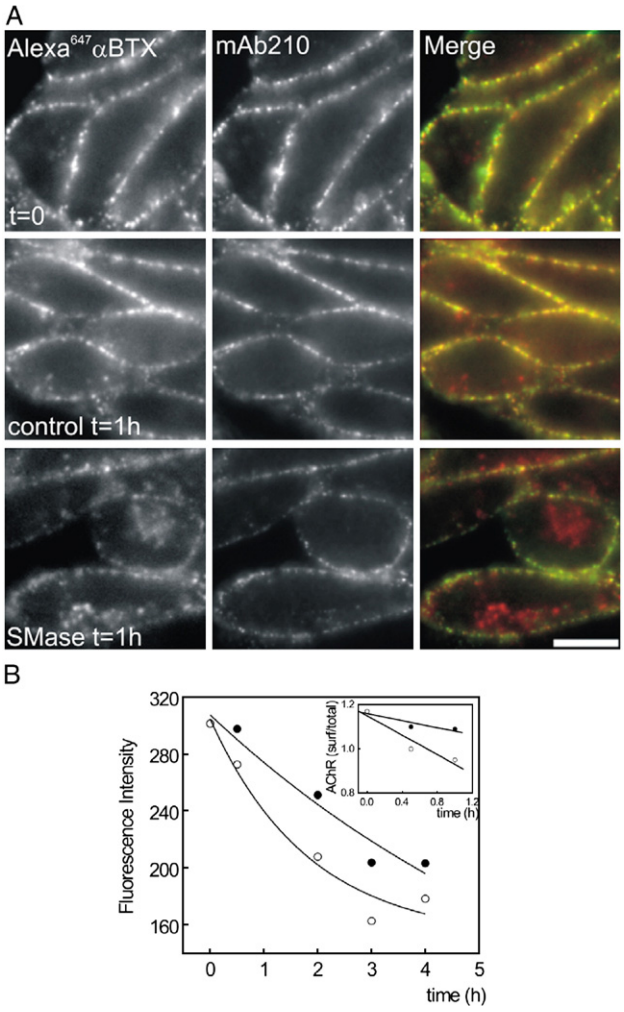

Fig. 7. *Cell-surface AChR diminution in SMase-treated cells is due to an enhanced internalization*. A) Fluorescence microscopy images following the internalization of plasma membrane AChR labeled with Alexa^{647}-αBTX in control and SMase-treated cells for the indicated times. Scale bar: 10 μm. B) Curves showing the decrease in Alexa^{488}-αBTX intensity of cell-surface labeled AChRs as a function of time for control (●) and SMase-treated cells (○). Inset: Internalization kinetics of AChR for the experimental conditions described in (B).

same extent as previously observed in CHO-K1/A5 cell upon Chol depletion [4].

3.8. Preincubation with nystatin enhanced the reduction in cell-surface AChR levels induced by SMase

In addition to SM hydrolysis, SMase treatment is reported to produce the rapid internalization of cell-surface Chol [53,54,22]. The possibility that the diminution in plasma membrane AChR by SMase was due to Chol internalization rather to SM depletion was therefore tested. For this purpose we incubated the cells with the sterol-binding antibiotic nystatin, which specifically interacts with and sequesters the plasma membrane Chol retained at the membrane [55]. Surface AChR levels decreased by ~30% upon nystatin treatment, similar to the extent observed in SMase-treated cells. When cells were incubated in the presence of both drugs, a further diminution (50%) in surface AChR levels resulted (Supplementary Fig. 4), indicating that SMase itself was effective in decreasing plasma membrane AChR even though Chol was not being internalized.

4. Discussion

Cer, intermediate molecules in the metabolism of sphingolipids, play an important role as second messengers for many cellular functions [56,36]. Cer associate with lipid "rafts" [57,58] and these Cer-enriched microdomains have been reported to spontaneously fuse into larger Cer-enriched membrane platforms [59–61]. Through these processes Cer appear to "catalyze" various signal transduction pathways recruiting membrane receptors and intracellular signaling molecules.

In the present study we examined the effects of short- and long-chain Cer on the AChR trafficking to the plasma membrane in a mammalian heterologous expression system, the CHO-K1/A5 cells. Most natural Cer have a long (16–24 C atoms) *N*-acyl chains, but short *N*-acyl chain Cer (2 C atoms) also occur in nature [35]. We found that low concentrations of exogenous C_6- or brain-Cer augmented the number of AChRs at the plasma membrane and decreased receptor levels at intracellular compartments (Fig. 1A–C). Recently Baier and Barrantes [8] showed that SLs are necessary for AChR assembly and trafficking to the plasma membrane in CHO-K1/A5 cells. Cer are key lipids in the metabolism of SLs. After a 2 h incubation of HL-60 cells with long-chain [^{14}C] C_{16}-Cer, most of the cell-bound radioactivity was found in free Cer and SM was the major metabolized SL containing labeled Cer [62]. Similar results were reported by Ridgway and Merrian [63] and Furuya et al. [64] using radiolabeled Cer that were converted into SM and GlcCer in CHO cells and in cerebellar neurons, respectively. Here, after 30 min incubation of CHO-K1/A5 cells with 5 μM C_6-Cer in the presence of trace concentrations of C_6-NBD-Cer, the production of C_6-NBD-SM was clearly observed (Fig. 1E). After 24 h incubation, the fluorescent Cer were completely converted to complex SL. Although the synthesis of complex SLs was tested only for C_6-Cer, long-chain Cer would be expected to behave similarly in the SL biosynthetic pathway [65]. Thus, low Cer treatment could contribute to augmenting the number of AChRs by an indirect mechanism, i.e. by enhancing the synthesis of SLs. We have recently demonstrated that the latter lipids play an important role in the regulation of AChR exocytic trafficking [8] and that addition of exogenous SMs results in increased levels of AChR at the cell surface [8].

The alteration in AChR distribution after low Cer treatment does not appear to be a general mechanism (Fig. 1D). Furthermore, the increment in cell-surface AChR levels produced by low Cer concentrations without changes in the surface levels of a predominantly "non-raft" membrane protein like VSVG-GFP [66] reinforces the importance of SLs for the correct trafficking of the AChR to the plasma membrane as recently proposed by Baier and Barrantes [8], and suggests the association of the AChR with lipid domains along the exocytic pathway.

The effect of higher Cer concentrations was also tested in the concentration range (between 25 and 37.5 μM) usually employed to study Cer effects on protein trafficking [23,67]. In this range, Cer markedly and specifically decreased the number of AChRs present at the plasma membrane with a concomitant increase in the intracellular receptor pool. Incubation of CHO-K1 cells (the cell line progenitor of the one used in the present study, CHO-K1/A5) with 25 μM C_6-Cer is reported to block the movement of VSVG through the *medial*- and *trans*-Golgi apparatus and its subsequent transport to the cell surface [23]. Short-chain Cer were reported to jam the transport of the scavenger receptor CD36 to the plasma membrane of monocytes and macrophages [67]. Analogously, high Cer concentrations could reduce cell-surface AChRs by blocking the exocytic traffic of newly synthesized receptors, as suggested by the changes in intracellular receptor distribution and its accumulation at the perinuclear region (Fig. 4B). More specifically, pEYFP-Gal-T and syntaxin 6, bona fide markers for the *trans*-Golgi/TGN [40,41], colocalized with Alexa Fluor^{647}-αBTX-labeled-AChR in large vesicular bodies generated by Cer treatment (Fig. 4B), reminiscent of the multivesicular bodies that Rosenwald and Pagano [23] characterized by electron microscopy. Exogenously added short-chain Cer are rapidly incorporated into cells and accumulate in the Golgi apparatus [30]. In CHO cells C_2-Cer decreased ARF-1 and PKC-α binding to Golgi-enriched membranes thereby preventing COP1 transport vesicle formation [68]. It was therefore possible that the blockade of AChR transport by exogenous Cer could affect in a more general manner the trafficking of proteins other than the AChR. This possibility was checked by transfecting CHO-K1/A5 cells with the fluorescent protein VSVG-GFP. We observed a significant (~45%) decrease in the GFP-fluorescence signal at the plasma membrane upon treatment with high C_6-Cer concentrations (Fig. 2D), indicating that a more general blockage of trafficking is operative at high Cer concentrations.

Besides the reduction in the AChR present at the plasma membrane, incubation with high C_6-Cer concentrations caused an increment in the affinity of the receptor for its canonical ligand, αBTX (Fig. 3A–D). Förster-type resonance energy transfer (FRET) studies from our laboratory showed that SMase digestion of *Torpedo* AChR-rich membranes generates Cer species with higher affinity for the receptor than the parental SM [69]. The increment in receptor affinity for the competitive

antagonist αBTX after Cer treatment observed here may result from changes in the biophysical properties of the cell membrane upon Cer treatment. Heron et al. [70] found that the increment in the microviscosity of the membranes resulted in an increment in the K_d of the serotonin receptor for its ligand. Long-chain Cer have been shown to increase lipid order in model membranes containing Chol [71]. In contrast, C_2- and C_6-Cer cause a concentration-dependent decrease in lipid order as measured by anisotropy of DPH-PC in plasma membrane vesicles isolated from RBL-2H3 mast cells [72].

Treatment of CHO-K1/A5 cells with SMase, which hydrolyzes plasma membrane SM with generation of endogenous Cer, also decreased cell-surface AChR levels and accelerated receptor endocytosis. This is in agreement with the reported reduction in CD36 expression resulting from SMase action on monocytes and macrophages [67]. In macrophages and fibroblasts SMase treatment induces formation of numerous vesicles that pinch off from the plasma membrane and internalize [34]. Acute Chol depletion from CHO-K1/A5 cells by methyl-β-cyclodextrin treatment dramatically accelerates AChR endocytosis [4]. The acceleration of the internalization kinetics by SMase is very similar to that resulting from Chol depletion by cyclodextrin [4], suggesting that both may result from a common disruption of Chol/SM-rich lipid domains. In the case of SMase action, this could produce the displacement of SM from such lipid domains by virtue of the higher affinity of the generated Cer for the AChR [69]. Long-chain Cer have the capacity to specifically displace sterol from lipid domains [22] and have been shown to require an N-linked acyl chain with at least 8 methylene units to displace Chol from SM-rich domains [73]. Interestingly, cell-surface Chol is rapidly internalized upon SMase action [53,54,22].

The possible synergism between SM and Chol in maintaining AChR cell-surface levels was further suggested by the nystatin experiments. Treatment with this sterol-binding antibiotic (which sequesters membrane-bound Chol but does not remove it from the plasma membrane, Supplementary Fig. 4), decreased AChR levels by ~30%. Preincubation with nystatin followed by SMase treatment in the continuous presence of the antibiotic showed a further diminution (~50%) in surface AChR levels, indicating that SMase was effective in decreasing plasma membrane AChR and suggesting that in addition to the key role played by Chol levels [4,5], SM is also involved in the stability of the plasma membrane-associated AChR. In summary, our results show that Cer were effective in modulating the trafficking of the AChR expressed in CHO-K1/A5 cells and that they exerted these effects in opposite ways and through different mechanisms depending on the lipid concentration.

Acknowledgments

This work was supported in part by grants from FONCYT, CONICET and UNS, Argentina, to F.J.B., and UNS to M.F.P.

Appendix A. Supplementary data

Supplementary data associated with this article can be found, in the online version, at doi:10.1016/j.bbamem.2007.10.019.

References

[1] F.J. Barrantes, Modulation of nicotinic acetylcholine receptor function through the outer and middle rings of transmembrane domains, Curr. Opin. Drug. Discov. Devel. 6 (2003) 620–632.
[2] F.J. Barrantes, Structural basis for lipid modulation of nicotinic acetylcholine receptor function, Brain Res. Rev. 47 (2004) 71–95.
[3] F.J. Barrantes, Cholesterol effects on nicotinic acetylcholine receptor, J. Neurochem. 103 (Suppl. 1) (2007) 72–80.
[4] V. Borroni, C.J. Baier, T. Lang, I. Bonini, M.W. White, I. Garbus, F.J. Barrantes, Cholesterol depletion activates rapid internalization of diffraction-limited acetylcholine receptor domains at the cell membrane, Mol. Membr. Biol. 24 (2007) 1–15.
[5] R. Kellner, C.J. Baier, K.I. Willig, S.W. Hell, F.J. Barrantes, Nanoscale organization of nicotinic acetylcholine receptors revealed by STED microscopy, Neuroscience 144 (2007) 135–143.
[6] M.F. Pediconi, C.E. Gallegos, E.B. De los Santos, F.J. Barrantes, Metabolic cholesterol depletion hinders cell-surface trafficking of the nicotinic acetylcholine receptor, Neuroscience 128 (2004) 239–249.
[7] A.M. Roccamo, M.F. Pediconi, E. Aztiria, L.P. Zanello, A. Wolstenholme, F.J. Barrantes, Cells defective in sphingolipids biosynthesis express low amount of muscle nicotinic acetylcholine receptor, Eur. J. Neurosci. 11 (1999) 1615–1623.
[8] C.J. Baier, F.J. Barrantes, Sphingolipids are necessary for nicotinic acetylcholine receptor export in the early secretory pathway, J. Neurochem. 101 (2007) 1072–1084.
[9] T.J. Proszinski, R.W. Klemm, M. Gravert, P.P. Hsu, Y. Gloor, J. Wagner, K. Kozak, H. Grabner, K. Walzer, M. Bagnat, K. Simons, C. Walch-Solimena, A genome-wide visual screen reveals a role for sphingolipids and ergosterol in cell surface delivery in yeast, PNAS 102 (2005) 17981–17986.
[10] A.G. Rosenwald, C.E. Machamer, R.E. Pagano, Effects of a sphingolipid synthesis inhibitor on membrane transport through the secretory pathway, Biochemistry 31 (1992) 3581–3590.
[11] S. Spiegel, D. Foster, R. Kolesnick, Signal transduction through lipid second messengers, Curr. Opin. Cell Biol. 8 (1996) 159–167.
[12] R.T. Dobrowsky, C. Kamibayashi, M.C. Mumby, Y.A. Hannun, Ceramide activates heterotrimeric protein phosphatase 2A, J. Biol. Chem. 268 (1993) 15523–15530.
[13] J. Liu, S. Mathias, Z. Yang, R.N. Kolesnick, Renaturation and TNFα stimulation of a 97 kDa ceramide-activated protein phosphatase, J. Biol. Chem. 269 (1994) 3047–3052.
[14] E. Gulbins, K.M. Coggeshall, G. Baier, D. Telford, C. Langlet, G. Baier-Bitterlich, N. Bonnefoy-Berard, P. Burn, A. Wittinghofer, A. Altman, Direct stimulation of Vav-guanine nucleotide exchange activity for ras by phorbol esters and diglycerides, Mol. Cell. Biol. 14 (1994) 4749–4758.
[15] J. Lozano, E. Berra, M.M. Municio, M.T. Díaz-Mecco, I. Domínguez, L. Sanz, J. Moscat, Protein kinase C isoform is critical for kappa B-dependent promoter activation by sphingomyelinase, J. Biol. Chem. 269 (1994) 19200–19202.
[16] G. Muller, M. Ayoub, P. Storz, J. Rannecke, D. Fabbro, K. Pfizenmaier, PKC ξ is a molecular switch in signal transduction of TNFα, bifunctionally regulated by ceramide and arachidonic acid, EMBO J. 14 (1995) 1961–1969.
[17] P.P. Ruvolo, Intracellular signal transduction pathways activated by ceramide and its metabolites, Pharmacol. Res. 47 (2003) 383–392.
[18] K. Simons, E. Ikonen, Functional rafts in cell membranes, Nature 387 (1997) 569–572.
[19] K. Simons, D. Toomre, Lipid rafts and signal transduction, Nat. Rev., Mol. Cell Biol. 1 (2000) 31–39.
[20] M. Edidin, The state of lipid rafts: from model membranes to cells, Annu. Rev. Biophys. Biomol. Struct. 32 (2003) 257–283.
[21] Y.J.E. Bjorkqvist, T.K.M. Nyholm, J.P. Slotte, B. Ramsted, Domain formation and stability in complex lipid bilayers as reported by cholestatrienol, Biophys. J. 88 (2005) 4054–4063.
[22] M. London, E. London, Ceramide selectively displaces cholesterol from ordered domains (rafts): implications for lipid raft structure and function, J. Biol. Chem. 279 (2004) 9997–10004.
[23] A.G. Rosenwald, R.E. Pagano, Inhibition of glycoprotein traffic through the secretory pathway by ceramide, J. Biol. Chem. 268 (1993) 4577–4579.

[24] J. Patrick, J. McMillan, H. Wolfson, J.C. O'Brien, Acetylcholine receptor metabolism in a nonfusing muscle cell line, J. Biol. Chem. 252 (1977) 143–153.
[25] W.N. Green, T. Claudio, Acetylcholine receptor assembly: subunit folding and oligomerization occur sequentially, Cell 74 (1993) 57–69.
[26] J. Schmidt, M.A. Raftery, A simple assay for the study of solubilized acetylcholine receptors, Anal. Biochem. 52 (1973) 349–354.
[27] O.H. Lowry, N.J. Rosebrough, A.L. Farr, R.J. Randall, A protein determination by the Folin-phenol reagent, J. Biol. Chem. 193 (1951) 265–275.
[28] D. Yildiz, N. Ercal, D.W. Armstrong, Nicotine enantiomers and oxidative stress, Toxicology 130 (1998) 155–165.
[29] Y. Fujii, T. Nomura, H. Kanzawa, M. Kameyama, H. Yamanaka, M. Akita, K. Setsu, K. Okamoto, Purification and characterization of enterotoxin produced by *Aeromonas sobria*, Microbiol. Immunol. 42 (1998) 703–714.
[30] N.G. Lipsky, R.E. Pagano, Sphingolipid metabolism in cultured fibroblast: microscopic and biochemical studies employing a fluorescent ceramide analogue, Proc. Natl. Acad. Sci. U. S. A. 80 (1983) 2608–2612.
[31] A. Loidl, R. Claus, H.P. Deigner, A. Hermetter, High-precision fluorescence assay for sphingomyelinase activity of isolated enzymes and cell lysates, J. Lipid Res. 43 (2002) 815–823.
[32] Y. Nakai, Y. Sakurai, A. Yamaji, H. Asou, M. Umeda, K. Uyemura, K. Itoh, Lysenin–sphingomyelin binding at the surface of oligodendrocyte lineage cells increases during differentiation in vitro, J. Neurosci. Res. 62 (2000) 521–529.
[33] E. Kiyokawa, T. Baba, N. Otsuka, A. Makino, S. Ohno, T. Kobayashi, Spatial and functional heterogeneity of sphingolipid-rich membrane domains, J. Biol. Chem. 280 (2005) 24072–24084.
[34] X. Zha, L.M. Pierini, P.L. Leopold, P.J. Skiba, I. Tabas, F.R. Maxfield, Sphingomyelinase treatment induces ATP-independent endocytosis, J. Cell Biol. 140 (1998) 39–47.
[35] J. Sot, F.M. Goñi, A. Alonso, Molecular associations and surface-active properties of short- and long-*N*-acyl chain ceramides, Biochim. Biophys. Acta 1711 (2005) 12–19.
[36] W.J. van Blitterswijk, A.H. van der Luit, R.J. Veldman, M. Verheij, J. Borst, Ceramide: second messenger or modulator of membrane structure and dynamics? Biochem. J. 369 (2003) 199–211.
[37] V. Kuhle, G.L. Abrahams, M. Hensel, Intracellular *Salmonella enterica* redirect exocytic transport processes in a *Salmonella* pathogenicity island 2-dependent manner, Traffic 76 (2006) 716–730.
[38] W. Hu, R. Xu, G. Zhang, J. Jin, Z.M. Szulc, J. Bielawski, Y.A. Hannun, L.M. Obeid, C. Mao, Golgi fragmentation is associated with ceramide-induced cellular effects, Mol. Biol. Cell. 16 (2005) 1555–1567.
[39] J.M. Mackenzie, M.K. Jones, E.G. Westaway, Markers for *trans*-Golgi membranes and the intermediate compartment localize to induced membranes with distinct replication functions in flavivirus-infected cells, J. Virol. 73 (1999) 9555–9567.
[40] B.E. Schaub, B. Berger, E.G. Berger, J. Rohrer, Transition of galactosyltransferase 1 from *trans*-Golgi cisterna to the *trans*-Golgi network is signal mediated, Mol. Biol. Cell 17 (2006) 5153–5162.
[41] F. Vandenbulcke, D. Nouel, J.P. Vincent, J. Mazella, A. Beaudet, Ligand-induced internalization of neurotensin in transfected COS-7 cells: differential intracellular trafficking of ligand and receptor, J. Cell Sci. 113 (2000) 2963–2975.
[42] T.A. Taha, Y.A. Hannun, L.M. Obeid, Sphingosine kinase: biochemical and cellular regulation and role in disease, J. Biochem. Mol. Biol. 39 (2006) 113–131.
[43] Y.A. Hannun, Functions of ceramide in coordinating cellular responses to stress, Science, 274 (1996) 1855–18599.
[44] A.F. Ross, M. Rapuano, J.H. Schmidt, J.M. Prives, Phosphorylation and assembly of nicotinic acetylcholine receptor subunits in cultured chick muscle cells, J. Biol. Chem. 262 (1987) 14640–14647.
[45] G. Sadasivam, R. Willmann, S. Lin, S. Erb-Vogtli, X.C. Kong, M.A. Ruegg, C. Fuhrer, Src-family kinases stabilize the neuromuscular synapse in vivo via protein interactions, phosphorylation, and cytoskeletal linkage of acetylcholine receptors, J. Neurosci. 25 (2005) 10479–10493.
[46] E.G. Bruneau, M. Akaaboune, The dynamics of recycled acetylcholine receptors at the neuromuscular junction in vivo, Development. 133 (2006) 4485–4493.
[47] M.A. Lanuza, R. Gizaw, A. Viloria, C.M. Gonzalez, N. Besalduch, V. Dunlap, J. Tomas, P.G. Nelson, Phosphorylation of the nicotinic acetylcholine receptor in myotube-cholinergic neuron cocultures, J. Neurosci. Res. 83 (2006) 1407–1414.
[48] T.A. Haystead, A.T.R. Sim, D. Carling, R.C. Honnor, Y. Tsukitani, P. Cohen, D.G. Hardie, Effects of the tumor promoter okadaic acid on intracellular protein phosphorylation and metabolism, Nature 337 (1989) 78–81.
[49] N.A. Bourbon, J. Yun, M. Kester, Ceramide directly activates protein kinase C zeta to regulate a stress-activated protein signaling complex, J. Biol. Chem. 275 (2000) 35617–35623.
[50] A. Yamaji-Hasegawa, A. Makino, T. Baba, Y. Senoh, H. Kimura-Suda, S.B. Sato, N. Terada, S. Ohno, E. Kiyokawa, M. Umeda, T. Kobayashi, Oligomerization and pore formation of a sphingomyelin-specific toxin, lysenin, J. Biol. Chem. 278 (2003) 22762–22770.
[51] R.E. Pagano, O.C. Martin, H.C. Kang, R.P. Haugland, A novel fluorescent ceramide analogue for studying membrane traffic in animal cells: accumulation at the Golgi apparatus results in altered spectral properties of the sphingolipid precursor, J. Cell Biol. 113 (1991) 1267–1279.
[52] D.A. Brown, E. London, Functions of lipid rafts in biological membranes, Annu. Rev. Cell Dev. Biol. 14 (1998) 111–136.
[53] J.P. Slotte, E.L. Bierman, Depletion of plasma membrane sphingomyelin rapidly alters the distribution of cholesterol between plasma membranes and intracellular cholesterol pools in cultured fibroblast, Biochem. J. 250 (1988) 653–658.
[54] N.D. Ridgway, Interactions between metabolism and intracellular distribution of cholesterol and sphingomyelin, Biochim. Biophys. Acta 1484 (2000) 129–141.
[55] P. Tewary, K. Veena, T.J. Pucadyil, A. Chattopadhyay, R. Madhubala, The sterol-binding antibiotic nystatin inhibits entry of non-opsonized *Leishmania donovani* into macrophages, Biochem. Biophys. Res. Commun. 339 (2006) 661–666.
[56] Y.A. Hannun, The sphingomyelin cycle and the second messenger function of ceramide, J. Biol. Chem. 26 (1994) 3125–3128.
[57] X. Xu, R. Bittman, G. Duportall, D. Heissler, C. Vilcheze, E. London, Effects of the structure of natural sterols and sphingolipids on the formation of ordered sphingolipids/sterol domains (raft), comparison of cholesterol to plant, fungal, and disease-associated sterols and comparison of sphingomyelin, cerebrosides, and ceramide, J. Biol. Chem. 276 (2001) 33540–33546.
[58] T.Y. Wang, J.R. Silvius, Sphingolipid partitioning into ordered domains in cholesterol-free and cholesterol-containing lipid bilayers, Biophys. J. 84 (2003) 367–378.
[59] J. Bock, I. Szabo, N. Gamper, C. Adams, E. Gulbins, Ceramide inhibits the potassium channel Kv1.3 by the formation of membrane platforms, Biochem. Biophys. Res. Commun. 305 (2003) 890–897.
[60] C.R. Bollinger, V. Teichgraber, E. Gulbins, Ceramide-enriched membrane domains, Biochim. Biophys. Acta 1746 (2005) 284–294.
[61] L. Silva, R.F. de Almeida, A. Fedorov, A.P. Matos, M. Prieto, Ceramide-platform formation and -induced biophysical changes in a fluid phospholipid membrane, Mol. Membr. Biol. 23 (2006) 137–148.
[62] D. Ardail, I. Popa, J. Bodennec, C. Famy, P. Louisot, J. Portoukalian, Subcellular distribution and metabolic fate of exogenous ceramides taken up by HL-60 cells, Biochim. Biophys. Acta 1583 (2002) 305–310.
[63] N.D. Ridgway, D.L. Merrian, Metabolism of short chain ceramide and dihidroceramide analogues in Chinese hamster ovary (CHO) cells, Biochim. Biophys. Acta 1256 (1995) 57–70.
[64] S. Furuya, J. Mitoma, A. Makino, Y. Hirabayashi, Ceramide and its interconvertible metabolite sphingosine function as indispensable lipid factors involved in survival and dendritic differentiation of cerebellar Purkinje cells, J. Neurochem. 71 (1998) 366–377.
[65] K. Venkataraman, A.H. Futerman, Comparison of the metabolism of L-*erythro*- and L-*threo*-sphinganines and ceramides in cultured cells and in subcellular fractions, Biochim. Biophys. Acta 1530 (2001) 219–226.
[66] T. Harder, P. Scheiffele, P. Verkade, K. Simons, Lipid domain structure of the plasma membrane revealed by patching of membrane components, J. Cell Biol. 141 (1998) 929–942.

[67] Y. Luan, H.R. Griffiths, Ceramides reduce CD36 cell surface expression and oxidised LDL uptake by monocytes and macrophages, Arch. Biochem. Biophys. 450 (2006) 89–99.
[68] A. Abousalham, T.C. Hobman, J. Dewald, M. Garbutt, D.N. Brindley, Cell-permeable ceramides preferentially inhibit coated vesicle formation and exocytosis in Chinese hamster ovary compared with Madin–Darby canine kidney cells by preventing the membrane association of ADP-ribosylation factor, Biochem. J. 361 (2002) 653–661.
[69] I.C. Bonini, S.S. Antollini, C. Gutierrez-Merino, F.J. Barrantes, Sphingomyelin composition and physical asymmetries in native acetylcholine receptor-rich membranes, Eur. Biophys. J. 31 (2002) 417–427.
[70] D.S. Heron, M. Shinitzkyt, M. Hershkowitz, D. Samuel, Lipid fluidity markedly modulates the binding of serotonin to mouse brain membranes, Proc. Natl. Acad. Sci. U. S. A. 77 (1980) 7463–7467.
[71] T.Y. Wang, J.R. Silvius, Different sphingolipids show differential partitioning into sphingolipid/cholesterol-rich domains in lipid bilayers, Biophys. J. 79 (2000) 1478–1489.
[72] A. Gidwani, H.A. Brown, D. Holowka, B. Baird, Disruption of lipid order by short-chain ceramides correlates with inhibition of phospholipase D and downstream signaling by FcεRI, J. Cell Sci. 116 (2003) 3177–3187.
[73] S. Nybond, Y.J. Bjorkqvist, B. Ramstedt, J.P. Slotte, Acyl chain length affects ceramide action on sterol/sphingomyelin-rich domains, Biochim. Biophys. Acta 1718 (2005) 61–66.